CHAPTER SIX

Elucidation Of Probable Mechanisms Of Configuration And Performance Of The Newly Fabricated Pore-Regulated Polymer Matrix Formulation Using Experimental And Computational Molecular Modeling Techniques

6.1. INTRODUCTION

In Chapter five, the potential toxicity and biocompatibility of the optimized P-RPM formulation was assessed utilizing tissue sample and mammalian cell cultures to undertake histopathological and cytotoxicity assays respectively. The outcome of these tests showed that both placebo and drug loaded P-RPM formulations were potentially non-toxic and biocompatible. Thus far, remarkable outcomes have been obtained from evaluating the efficiency of the P-RPM formulation. Therefore, it is also necessary to attempt to evaluate, comprehend and explicate the possible mechanisms guiding the formation and perfomance of this novel drug delivery system.

The systematic elucidation of possible mechanisms guiding the formation and action of the newly fabricated P-RPM formulation intends to provide valuable information that may be applied to the modification of this system or even the adapted invention and construction of other novel porosity-enabled drug delivery devices. The measurement of relevant physicochemical and physicomechanical quantities could give a lead to understanding and been able to propose the mechanistics guiding the configurative design and performance of the optimized P-RPM formulation.

Computational molecular modeling and structural rationalization techniques are becoming fundamental to the innovations of pharmaceutical sciences with the main goal of rational drug discovery, development of biomaterials and delivery systems design especially those that were previously unexplored due to their complex nature and shortage of interdisciplinary expertise required to invent the computational models of various phenomenon (Haworth, 2006; Sibeko *et al*., 2009). A computational model can be described as a mathematical model that requires extensive computational resources to systematically study, predict or provide an insight to the complex behaviour of an entity or system utilizing a minimum number of experimental studies.

The combination of polymer and pharmaceutical sciences with computational molecular modeling has resulted in the integration of theoretical scientific facts into efficient computer software to gain further insight into the complexity and behaviour of the newly developed material. This provides a justification of theoretical concepts when conclusive postulations correlate well with experimental data (Sibeko *et al*., 2009). Computational modeling uses

molecular and quantum mechanics such as semi-empirical, *ab initio* and density functional theory to predict the molecular structural make-up of systems, compute varying molecular descriptors or reveal underlying physical trends governing the performance of a system that may not be revealed by laboratory experiments. With regards to the level of relevance of computational modeling, it can be described as a third component of the research triad complementing experiment and theory (Sibeko *et al*., 2009).

Computational modeling has been extensively employed as an efficient tool in the design, comprehension and prediction of mechanisms guiding the design and functioning of drug delivery systems. Some examples of such applications include but are not limited to simulation of drug release from microspheres (Arifin *et al*., 2006; Abdekhodaie and Wu, 2008), intravitreal drug delivery (Kathawate and Acharya, 2008), nasal drug delivery systems (Kleven, 2005; Inthavong *et al*., 2008), intratumoral drug delivery (Ward and King, 2003; Weinberg *et al*., 2007; Altinok *et al*., 2009), central nervous system drug delivery (Allen and Geldenhuys, 2006), intravaginal drug delivery (Ndesendo *et al*., 2009), colonic drug delivery (Waterman and Sutton, 2003), transdermal drug delivery (Ouriemchi and Vergnaud, 2000; Naegel, *et al*., 2008) and implantable devices (Collins, 1998).

The object of this Chapter was to attempt to elucidate the mechanisms guiding the formation and performance of the newly developed optimized P-RPM formulation utilizing both experimental and computational modeling approaches. This achieved by conducting experiments such as Fourier transform infrared spectroscopy, temperature modulated differential scanning calorimetry, gravimetric weight determinations, quantitative matrix porosity, microscopic surface morphological assessments, matrix dissolution and erosion evaluations and measurement of related physicomechanical quantities. Additionally, semi-empirical quantum mechanics was employed to generate computational models and energy paradigms to predict underlying mechanisms of matrix configuration and function. The PS loaded P-RPM formulation was utilized as a model for this phase of the study to ensure that this set of investigations is systematically approached.

6.2. EXPERIMENTAL SECTION

6.2.1. Materials

The optimized PS loaded P-RPM formulation and the corresponding homogenous co-particulate blend employed for its fabrication discussed in Chapters two and three were employed for this part of the investigation. All other materials used are the same as in Chapters two and three (Sections 2.2.1 and 3.2.1).

6.2.2. Experimental approach to the elucidation of the mechanisms of configuration and function of the P-RPM formulation

6.2.2.1. Mechanism of configuration/formation

6.2.2.1.1. Assessment of possible structural transitions during matrix preparation

The FTIR spectra for the non-lyophilized homogenous co-particulate blend and lyophilized porous matrix loaded with PS were recorded on the Perkin Elmer Spectrophotometer (Section 4.2.3). 10mg of each formulation was placed on the sample holder situated on the machine stage. All other procedural steps taken were same as those already described in Chapter four (Section 4.2.3).

6.2.2.1.2. Determination of thermal behaviour using differential scanning calorimetry

The thermal properties of the non-lyophilized homogenous co-particulate blend, lyophilized porous matrix loaded with PS and each compound employed in the fabrication of the drug-loaded P-RPM formulation were analyzed using the conventional differential scanning calorimetry (C-DSC). In addition, temperature modulated differential scanning calorimetry (TM-DSC) was only applied to the non-lyophilized homogenous co-particulate blend and lyophilized porous matrix loaded with PS to visualize important hidden transitions as both systems can be described as “multi-component” or “complex”. All DSC curves were recorded in triplicate on a DSC1, STAR^{e} System equipped with computational software for analysis (Mettler Toledo, Switzerland) employing 5mg of the respective samples placed in crimped aluminium pans. For the C-DSC determinations, the non-lyophilized homogenous blend was heated within the range of -35 to 500°C while the constituting chemical compounds and lyophilized porous matrix were heated from -35 to 350°C at a rate of 10˚C/min under inert nitrogen as a purging gas.

Temperature modulated DSC (TM-DSC) measurement was conducted using:

- a heating rate of 1˚C/minute for a period of 60 seconds
- a modulation amplitude of 0.8˚C
- a loop increment and segment of 0.8 and 1 respectively
- an automatically computed count of 212 over a selected temperature ranges.

The curves generated were smoothed at an order of 1 to 200 points and all experiments were carried out in triplicate. The temperature ranges employed for the respective samples are stated as follows:

(i) *Non-lyophilized homogenous blend*

- -35 - 55°C
- 60 - 140°C
- 145 - 300°C
- 305 - 450°C

(ii) *Lyophilized pore-regulated polymer matrix*

- 0 - 120°C
- 150 - 260°C

The above listed temperature ranges were selected as these were the segments within which salient thermal activities had occurred.

6.2.2.1.3. Changes in sample weight before and after lyophilization

Respective samples were weighed at different phases in the preparation of the P-RPM formulation. This included dry mixture before addition of ethanol and water for homogenization (S0), homogenous co-particulate blend (S1), blend stored away for curing (S2), pre-frozen blend after curing (S3), blend after 24 hour lyophilization cycle (S4) and completely lyophilized (after 48 hours) P-RPM formulation (S5). All measurements were done in triplicate employing a laboratory weighing balance (Mettler Toledo, AB104-S, Microsep Pty Ltd, Switzerland).

6.2.2.1.4. Evaluation of the physicomechanical texture

Textural analysis was used to quantify the variations in physicomechanical strength of measurable samples which were the water-based and ethanol-based co-particulate dispersions, non-lyophilized co-particulate homogenous blend before and after curing and the lyophilized P-

RPM formulation. The values obtained from these samples were compared to dry mixture of the constituting compounds and model drug. For easy and relatively accurate measurement, this mixture was placed in a plastic tub and subjected to physicomechanical testing. The parameters measured included the matrix firmness (M_F) and energy of matrix distortion ($Є_D$). Other experimental stipulations undertaken were the same as those described in Chapter two (Section 2.2.11).

6.2.2.2. Mechanism of function/action

In an attempt to visualize and elucidate the possible mechanisms guiding matrix performance, P-RPM formulations were separately placed into 25mL of simulated saliva of pH 6.8 contained in closed 100mL capacity glass jars maintained at 37±0.5^{o}C and 20rpm in a shaking incubator (Orbital Shaker Incubator, LM-530, Lasec Scientific Equipment, Johannesburg, South Africa). At specified time intervals (1, 2, 4 and 8 hours) remnants of sample placed in dissolution media were taken out, air dried to a constant weight, analysed and compared with the intact P-RPM formulation. Each set of experiment were conducted in triplicate. Each sample set were represented as follows:

- **X_{0hr}** – P-RPM formulation not exposed to the dissolution media
- **X_{1hr}** – P-RPM formulation after 1 hour exposure to dissolution media
- **X_{2hr}** – P-RPM formulation after 2 hour exposure to dissolution media
- **X_{4hr}** – P-RPM formulation after 4 hour exposure to dissolution media
- **X_{8hr}** – P-RPM formulation after 8 hour exposure to dissolution media

These samples were analysed employing the following techniques:

6.2.2.2.1. Infrared Spectrophotometry

About 10mg sample size was analysed with the Perkin Elmer FTIR Spectrophotometer (Section 4.2.3. In this case, the methodology explained in Section 6.2.2.1.1 was employed.

6.2.2.2.2. Scanning electron microscopy

The surface morphological changes of samples X_{0hr} – X_{8hr} were viewed under a JSM-840 Scanning Electron Microscope (JEOL 840, Tokyo, Japan) at a voltage of 20 keV and a magnification of 1000×. Samples (2mm diameter × 2mm thickness) were sputter-coated with gold-palladium and viewed six times from different angles.

6.2.2.2.3. Gravimetric analysis

In vitro matrix erosion trends were assessed by measuring the weight of each sample (X_{0hr} – X_{8hr}). All determinations were done in triplicate and the mathematical expression defined in Equation 6.1 was employed to determine the fractional mass loss in $^{w}/_{w}$.

$$\text{Fractional Mass Loss} = \frac{\text{Original Mass} - \text{Residual (dry) Mass}}{\text{Original Mass}} \qquad \textit{(Equation 6.1)}$$

6.2.2.2.4. Textural Analysis

Changes in matrix physicomechanical strength were measured in terms of matrix firmness (M_F) and energy of matrix distortion ($Є_D$) using textural profiling analysis. The methodology explained in Chapter two (Section 2.2.11) was utilized.

6.2.3. Prediction of the underlying mechanisms of configuration and function of the P-RPM with computational modeling

The overall performance of the pore-regulated matrix formulation being investigated is dependent on complex mechanisms of formation and function of its three-dimensional porous structure. Consequently, chemometric and structural computational modeling approach was employed to evaluate and predict these underlying mechanisms of matrix configuration and function as well as substantiate the experimental findings. In addition, semi-empirical quantum mechanics were employed to generate molecular interactions and computational energy paradigms of the porous matrix components based on inherent interfacial homogenization and lyophilization phenomena underlying the mechanisms of formation and action as provided by the co-particulate blend and solid state porous matrix. Models and graphics supported on the step-wise mechanistic molecular transitions were generated in our laboratory using the ACD/I-Lab, V5.11 (Add-on) software (Advanced Chemistry Development Inc., Toronto, Canada, 2000).

6.3. RESULTS AND DISCUSSION

6.3.1. Experimental techniques for the explication of fundamental mechanisms of formation and action of the P-RPM formulation

6.3.1.1. Mechanism of formation/configuration

6.3.1.1.1. Examination of probable shifts in frequency bands of pertinent functional moieties

Distinctive functional moieties with respective characteristic vibrational frequencies of the pure polymeric, non-polymeric compounds and model drug, PS contained in the P-RPM formulation were identified from their generated FTIR spectra. Relevant recorded bands are enlisted in Table 6.1 (Silverstein and Bassler, 1991; Taylor and Zografi, 1997; Van den Mooter *et al*., 2001; Sethia and Squillante, 2004; Kolawole *et al*., 2007). Subsequently, possible changes in band frequencies of these salient structural measures were compared with the FTIR spectra of the homogenous co-particulate blend (before lyophilization) and the lyophilized P-RPM formulation. FTIR spectra generated for the PS loaded un-lyophilized homogenous co-particulate blend and lyophilized pore-regulated formulation is illustrated with Figures 6.1 and 6.2. The FTIR spectra of the un-lyophilized, homogenous co-particulate blend and lyophilized P-RPM formulation showed that both matrices/systems are made up of several compounds as common bands overlapped while some shifted in terms of their frequencies and transmittance intensities due to the impact of other compounds present within the same system.

The FTIR spectra of the un-lyophilized blend displayed in Figure 6.1 displayed a broad band at 3272cm^{-1} which may be attributable to the overlap of the OH and NH_2/NH or C-OH stretching vibrations present in all components as reflected in Table 6.1 or the influence of the presence of multiple intra- and intermolecular hydrogen bonds due to the introduction of the ethanol and water for the dispersions of the solutes. This may have resulted in the hydration of the component compounds or hydrolysis of the C-O$^-$ Na$^+$ from PS The bands at 2981 - 2920cm^{-1} could be related to C-H stretching from the methylene (-CH_2-) or ethoxide (-O-C_2H_5) functional groups and C-H stretching/bending of alkyl groups respectively. The peak at 2158cm^{-1} may be an extension of the effects of the C-H and O-C_2H_5 vibrations which was influenced by the introduction of the solvents, ethanol and water. The peaks recorded at 1641 - 1413cm^{-1} are characteristic of overlapping vibrations from C-OH and N-H bending; NH_2 and NH_3^+ deformations; C=O, C-N, C=C, C-O-C, COO^- and O^-Na^+ stretches as well as weak phenyl C=C overtones from the different compounds. Furthermore, the bands recorded at 1084 - 1044cm^{-1} are notable for interactions of C-O, C-N, C-OH (acyclic), C-OH and C-O-C (linear) stretching vibrations as well as C-H (out-of-plane) deformations. Finally, the band recorded at 877cm^{-1} could be associated with non-destructive, reversible, physical perturbations of the structural backbones of some components due to solvation with functional group vibrations such as N-H

and C-OH deformation, O-C=O and N-C=O bending occurring (Silverstein and Bassler, 1991; Taylor and Zografi, 1997; Van den Mooter *et al*., 2001; Sethia and Squillante, 2004; Kolawole *et al*., 2007).

With respect to the spectra generated for the lyophilized P-RPM formulation, several peaks were also observed due to the contributive influences of its components compounds. Notable peaks were observed at 3510 - 3232cm^{-1} associated with OH, NH and NH_2 stretches; 3064 - 2854cm^{-1} attributable to interactive C-H (cyclic or linear), intramolecular hydrogen bonded NH_2 and OH stretch, O-C_2H_5 bending; 2155cm^{-1} due to weak C-H combinatorial overtones within the benzene ring; 1780 - 1724cm^{-1} due to C=O, C=C stretching, -NH_3^+ and NH_2 deformations, N-H bending vibrations; 1557 - 1445cm^{-1} consequent to COO^-, C-O-C (linear/acyclic), C-N stretching, C-OH in-plane bend, C-O^- and CH deformation; 1291 - 1082cm^{-1} resulting from C-OH (acyclic and cyclic), C-O-C (acyclic), C-N stretching; 915 - 677cm^{-1} associated with C-OH, NH deformations, O-C=O, N-C=O and C-OH (out-of plane) bending (Silverstein and Bassler, 1991; Taylor and Zografi, 1997; Van den Mooter *et al*., 2001; Sethia and Squillante, 2004; Kolawole *et al*., 2007). Furthermore, the absence of the conspicuous broad band observed for the un-lyophilized blend (Figure 6.1) between 3300 - 4000 cm^{-1} reflects the absence of OH and NH_2 functional moieties from the presence of water due to lyophilization process.

The observed trends of peaks for both un-lyophilized and lyophilized systems highlight that structural transitions were physical in nature and that the shifts recorded for characteristic peaks were probably due to the reversible interactions between the constituting compounds of the formulation. Also, formation of reversible, non-destructive hydrogen bonds during the solute dispersion process with ethanol/water combination may also have influenced the shifts in measured frequencies. Furthermore, the lyophilization process which involved the process of converting solidified solvent (pre-freezing) to gas (sublimation) to form the porous networks may initiate physical interactive intra- and intermolecular forces such as the van der Waals, electrostatic, ionic types which may also instigate observed frequency shifts. Overall, the processes (interphase, co-particulate, co-solvent, homogenization technique, pre-freezing and lyophilization) employed in the fabrication of the P-RPM formulation did not result in the destruction of the chemical backbone structure of the constituting compounds. In other words, each constituting compounds retained their original physicochemical and physicomechanical properties during the construction of the P-RPM formulation.

Table 6.1: A presentation of the vibrational frequencies and functional moieties of the respective pure compounds constituting the P-RPM

Compound	Functional Groups	Vibrational Frequencies (cm^{-1}) and Remarks
Chitosan	$-CH_2OH$	2883 (CH stretch), 3442 (OH stretch), 1036 (C–OH stretch)
	-C-O-C	1158 (C-O-C cyclic stretch)
	$-NH_2$	3421 (NH stretch), 1611 ($-NH_2$ deformation)
Menthol	$-CH_3$	2930 (CH stretch), 1449 (CH anti-symmetric deformation), 1371 (CH symmetric deformation)
	Cyclic CR_2OH	3264 (OH stretch), 1446 (C-OH in-plane bend), 682 (C-OH out-of-plane deformation)
Gelatin	$-CONH_2$	3334 (overlapping NH_2 and NH stretch), 1634 (C=O stretch), 1616 (NH_2 deformation), 1428 (C-N stretch)
	-CONHR	1542 (NH bend), 1250 (C-N stretch)
	$-CONR_2$ (*R= C atoms from a cyclic ring*)	620 (N-C=O bend)
	$-C-NH_3^+ - COO^-$	3018 (H-bonded NH_2 and OH stretch), 1501 ($-NH_3^+$ deformation), 1495 (COO^- stretch)
	$-CH_2-$	2986 (C-H) stretch
Polyvinyl alcohol	$-CH_2-$	2952 (C-H stretch)
	$-CR_2OH$	3380 (OH stretch), C-OH (1101), 1086 (C-O-C stretch)
Magnesium stearate	$-CH_2-$ (multiple, linear chain)	2921, 2928 (C-H stretch)
	$-COO^- - Mg^{2+} - COO^-$	1579, 1577 (C=O stretch), 3481 ($O^- Mg^+$ stretch), 1122 (C-O stretch)
Sorbitan ester 80	CR_2OH	3538 (OH stretch), 1098 (acyclic C-OH stretch),1118 (cyclic C-OH stretch)
	C-O-C (cyclic)	1179 (C-O-C stretch)
	C=O	1744 (C=O stretch)
	-HC=CH-	3024 ($=CH_2$ stretch), 1645 (C=C stretch), 1178 (C-H out-of-plane deformation)
Carbopol 974P NF	-COOH	3185 (H-bonded OH stretch), 1707 (C=O stretch), 942 (C-OH deformation), 756 (O-C=O bend)
Ethylcellulose 10	CR_2OH (R = cyclic moiety)	3533 (OH stretch), 1065 (C-OH stretch)
	-C-O-C (within a ring)	1380 (C-O-C stretch)
	$O-C_2H_5$	2980 (bending)
Hydroxyethylcellulose	C-O-C (cyclic)	1439 (C-O-C stretch)
	C-O-C (linear)	1135 (C-O-C stretch)
	C-OH (cyclic)	1062 (C-OH stretch)
	$C-OC_2H_5$	3462 (OH stretch), 2921 (C-H stretch)
Phenytoin sodium	C_5H_6	3154 (C-H stretch), 1693-2018 (weak C-H from the benzene/phenyl ring; overtones and combinations)
	$R_2-C=O$	1693 (C=O stretch)
	R-NH-	3341 (NH stretch), 1159 (C-N stretch), 697 (NH deformation)
	$-O^- Na^+$	1401 (stretch)

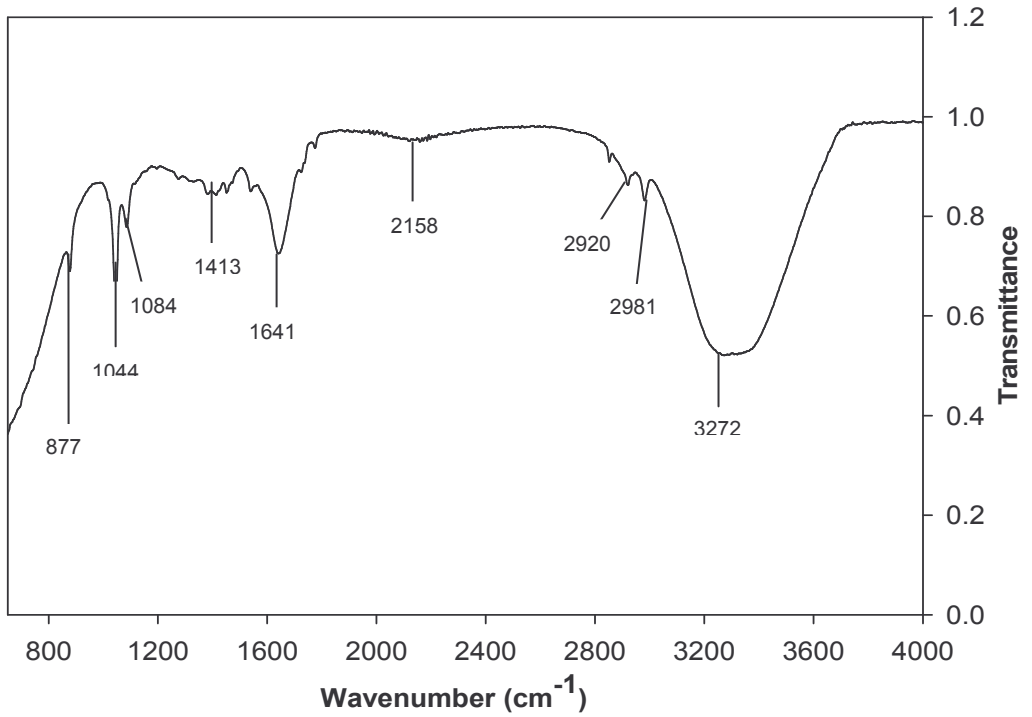

Figure 6.1: FTIR spectra of the optimized, un-lyophilized co-particulate homogenous blend loaded with PS.

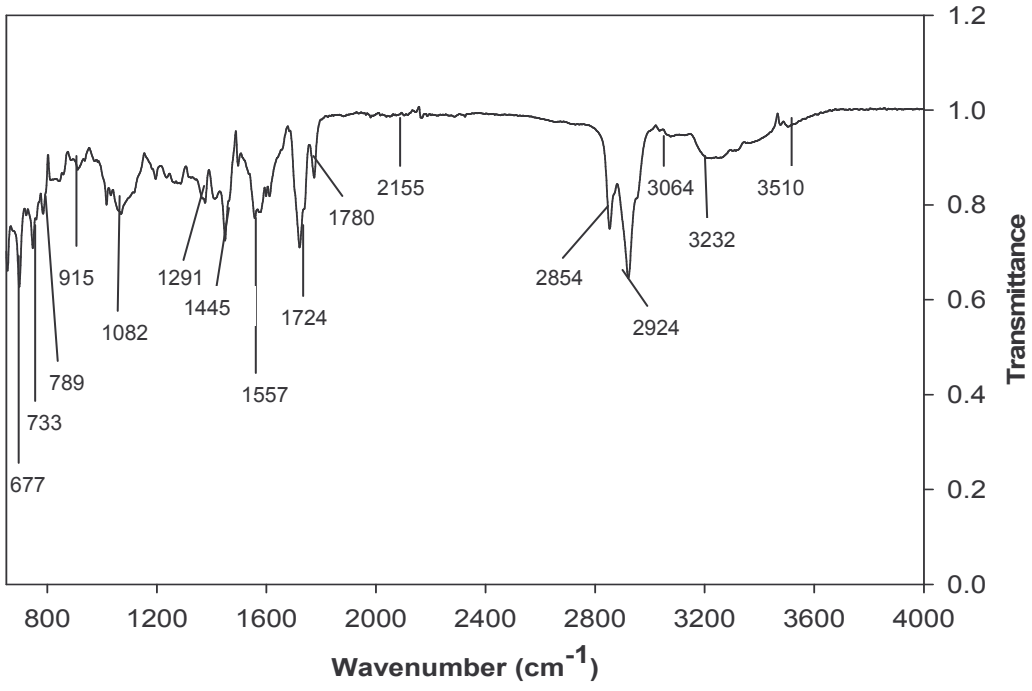

Figure 6.2: FTIR spectra of the optimized, lyophilized P-RPM formulation loaded with PS.

6.3.1.1.2. Changes in thermal quantities due to the application of heat energy

The thermal transitions which occurred within the un-lyophilized homogenous blend and lyophilized P-RPM formulation lattices were measured in terms of the glass transition (T_g) measured as the reversible heat flow due to changes in the magnitude of the heat capacity complex (C_p-complex) values (ΔC_p) and melting (T_m) temperature peaks which are as a result of irreversible heat flow processes corresponding to the total heat flow readings. In addition, the thermal reactivity of the pure constituting compounds and model drug, PS, was also assessed in terms of T_g and T_m using C-DSC so as to make reasonable comparisons with the un-lyophilized homogenized blend and lyophilized P-RPM formulation. The values obtained from the C-DSC and TM-DSC thermograms are presented in Table 6.2.

Table 6.2: Measured glass transition and melting temperature values for the pure compounds employed in the fabrication of the P-RPM formulation using C-DSC

	Salient Temperature Transition Points (°C)	
Pure Compounds	**T_g** [a]	**T_m** [b]
Chitosan	55.08	222.54
Menthol	44.11	212.89
Gelatin	60.99	228.87
Polyvinyl alcohol	48.56	210.03
Magnesium stearate	80.04	202.12
Span 80	60.01	260.33
Carbopol 974	67.96	218.47
Ethylcellulose 10	101.02	228.68
Hydroxyethylcellulose	87.97	234.55
Phenytoin sodium	85.99	200.05

T_g = Glass transition temperature and T_m = Melting temperature

Temperature modulated DSC involved sinusoidal temperature modulations with constant heating and cooling rates typified by short and small amplitudes and was able to reveal and distinguish important hidden and overlapping thermal events which the C-DSC did not identify. Figures 6.3 and 6.4 show the TM-DSC profiles at the different heating temperature ranges for the un-lyophilized homogenous co-particulate blend and the lyophilized P-RPM formulation respectively.

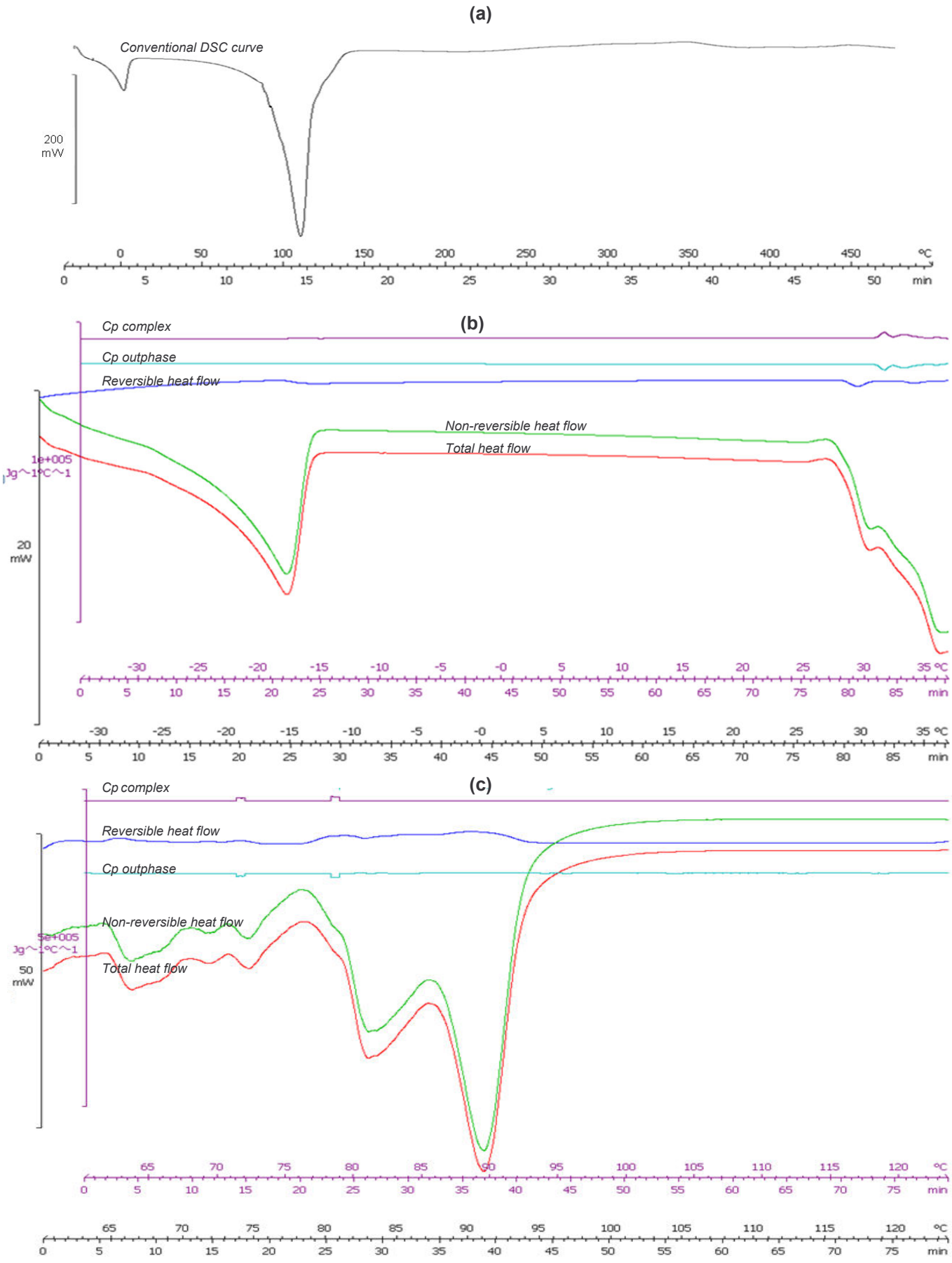
(a)
Conventional DSC curve
200
mW
0 50 100 150 200 250 300 350 400 450 °C
0 5 10 15 20 25 30 35 40 45 50 min
(b)
Cp complex
Cp outphase
Reversible heat flow
Non-reversible heat flow
Total heat flow
1e+005
Jg^-1°C^-1
20
mW
-30 -25 -20 -15 -10 -5 -0 5 10 15 20 25 30 35 °C
0 5 10 15 20 25 30 35 40 45 50 55 60 65 70 75 80 85 min
(c)
Cp complex
Reversible heat flow
Cp outphase
Non-reversible heat flow
Total heat flow
5e+005
Jg^-1°C^-1
50
mW
65 70 75 80 85 90 95 100 105 110 115 120 °C
0 5 10 15 20 25 30 35 40 45 50 55 60 65 70 75 min

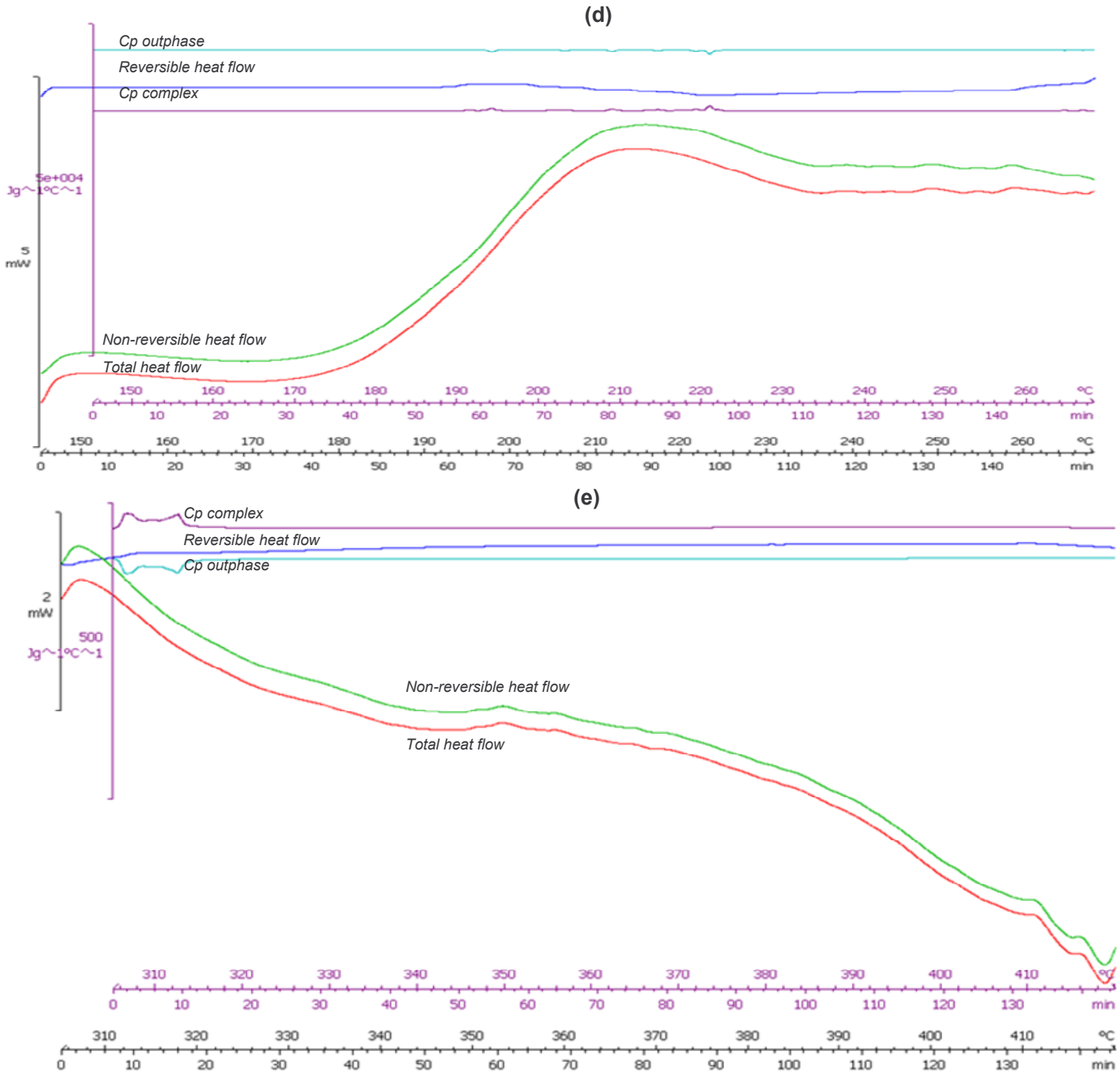

Figure 6.3: Different thermograms of the un-lyophilized homogenous co-particulate blend showing the: (a) C-DSC curve, (b), (c), (d) and (e) TM-DSC curves with the endothermic and exothermic peaks generated from the reversible, non-reversible and total heat flows at varying temperature ranges.

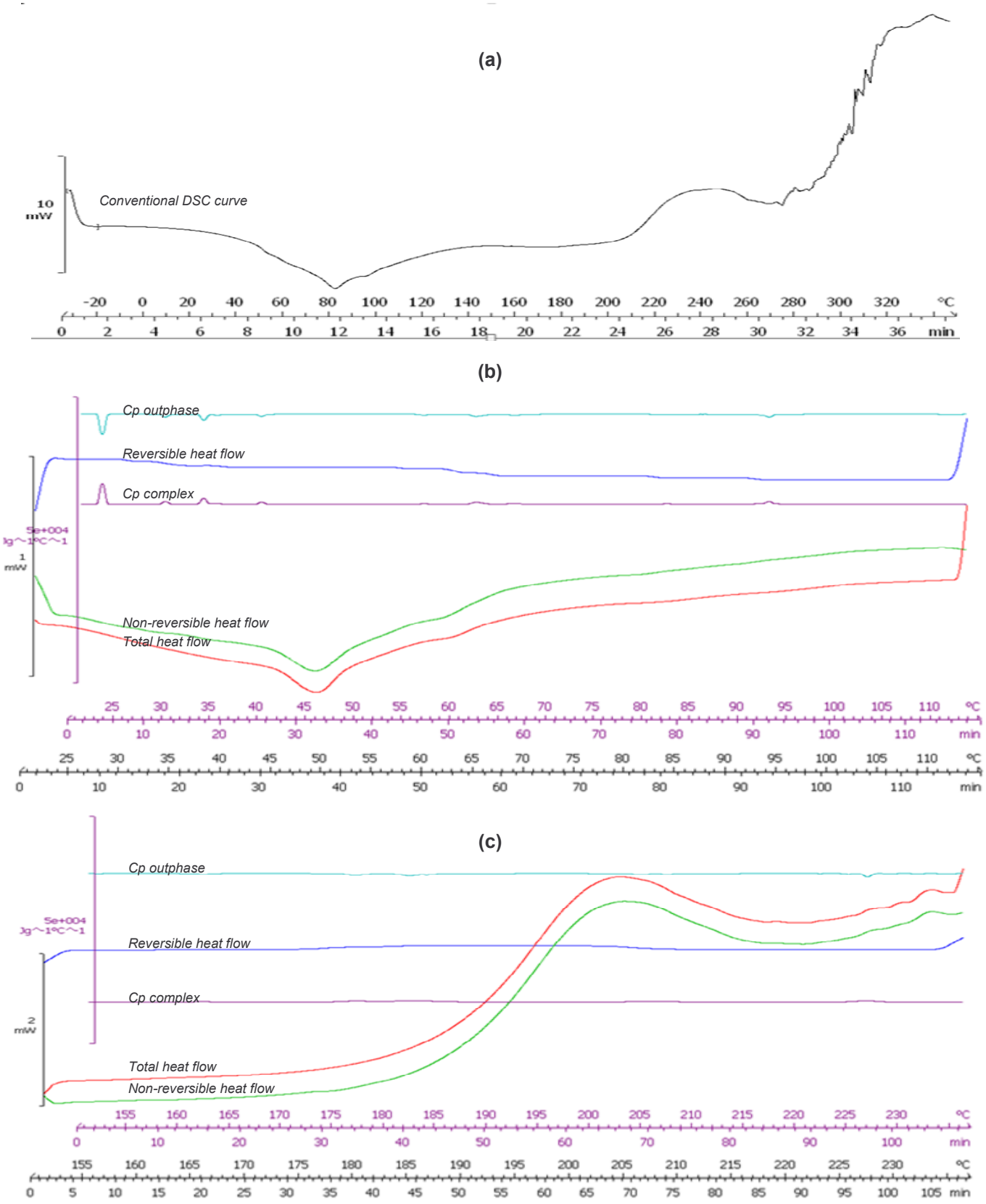

Figure 6.4: Diversified thermograms of the lyophilized P-RPM formulation showing the: (a) C-DSC curve, (b) and (c) TM-DSC curves with the endothermic and exothermic peaks generated from the reversible, non-reversible and total heat flows at specific temperature cycles.

The un-lyophilized homogenous blend and lyophilized P-RPM formulation displayed multi-transitional thermal behaviours as several T_g and T_m peaks were recorded (Table 6.3).

Table 6.3: Temperature changes revealing salient multi-transitional thermal events evidenced by diverse endothermic and exothermic inflection peaks

Thermal Events	Homogenous Blend	P-RPM Formulation
Glass Transition Temperature (T_g) (°C)		
	-17.54	24.11
	-14.25	28.49
	30.44	33.00
	64.55	39.61
	71.52	56.04
	89.59	61.00
	190.50	65.42
	202.00	83.00
	210.11	94.01
	215.98	161.54
	218.00	177.22
	221.15	182.00
	262.02	205.11
	264.08	227.00
	307.59	
	310.09	
Melting Temperature (T_m) (°C)		
	-14.09	23.15
	30.55	45.50
	36.00	59.91
	63.00	80.05
	69.00	180.22
	73.11	218.04
	81.50	
	89.84	
	173.30	
	238.52	
	252.99	
	264.00	
	342.01	

The existence of multiple thermal activity peaks, namely the glass transition (endothermic) and melting (exothermic) temperatures, indicate the presence of a combination of different compounds within the matrices (i.e. un-lyophilized homogenous blend and the lyophilized P-RPM formulation) investigated. In other words, this indicates the absence of any irreversible chemical transformation during the preparation of the P-RPM formulation implying that these procedures (interphase, co-particulate, co-solvent, homogenization technique, pre-freezing and lyophilization) involved reversible, physical transitions. However, a comparison of the T_g and T_m numerical values of the pure compounds (Table 6.2) and the mixture (Table 6.3) makes it obvious that the combination of the different compounds as well as the introduction of water and ethanol resulted in shifts in the T_g and T_m values.

Thus, the multiple thermal peaks exhibited and the collective differences observed in the thermal behaviors of the un-lyophilized homogenous blend and the lyophilized P-RPM formulation could be due to the contributive influence of the individual component of each system. As regards the un-lyophilized homogenous blend, the presence of interactive intra- and inter-molecular hydrogen bonding due to the presence of water and ethanol molecules may play a major role in influencing T_g and T_m values. The presence of multiple compounds within the P-RPM matrix as well as the presence of water and ethanol molecules in the un-lyophilized blend influenced dominant dynamical physical processes governing non-destructive structural mobility which may be responsible for the peak shifts recorded in Table 6.3. Therefore, this could have an influence on the extent of matrix distortion, chain structural relaxation and entropy changes within each lattice. This could eventually have influenced the dynamic dimensional changes as a result of chain realignments and rearrangements (glass transition), bond breakages and chain deformations (melting), which may affect the thermodynamic stability of both systems during the process of heating giving rise to the differences in magnitudes of the measured thermal quantities (Table 6.3).

Furthermore, the total heat energy required to bring about the observed thermal transitions (T_g and T_m) were computed utilizing mathematical integration. The un-lyophilized blend had higher values (200.16mJ) than the P-RPM (10.08mJ) attributable to the presence of water and ethanol in the blend resulting in the formation of multiple hydrogen bonds which need to be dissociated before any macroscopic dimensional entropic changes could be realized. Therefore, the blend

required higher thermal energy than lyophilized P-RPM formulation to induce inter-polymeric transitional motions required for the glass transition and melting thermodynamic processes.

6.3.1.1.3. Gravimetric changes of samples during the process of fabrication of the P-RPM formulation

The changes in weight at the different phases of constructing the P-RPM formulation are illustrated with Figure 6.5.

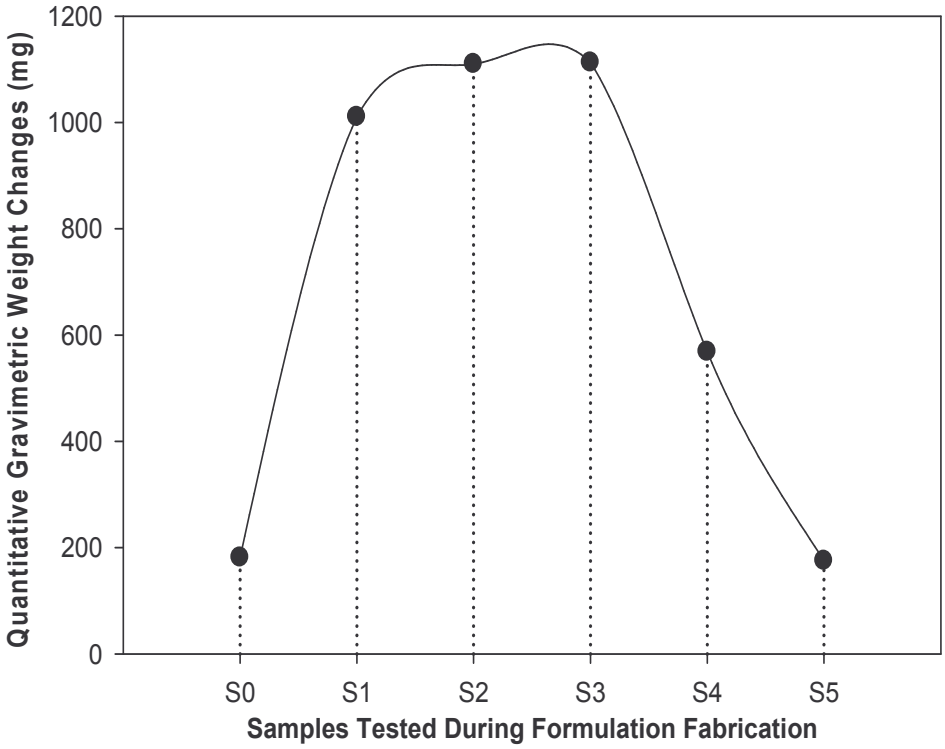

Figure 6.5: Quantification of gravimetric weight changes at strategic points during the fabrication of the P-RPM formulation (n = 3 and Standard Deviation ≤ 8.95mg in all cases).

The trend of weight changes can be partitioned into four phases which includes an initial increase from S0 to S1; a relatively constant segment from S1 to S2, a slight increase from S2 to S3 followed by a sharp decrease at S4 and S5. An increase in weight observed from S0 (181.50 ± 3.45mg) to S1 (1010.51 ± 7.06 mg) was due to the additive densities/masses/volumes of span 80, water and ethanol introduced to form the homogenous co-particulate blend. The

weight of S1 (1010.51 ± 7.06 mg) was maintained after the process of curing the blend in the dark (S2: 1109.89 ± 5.11mg) indicating that this process served only to enhance physical homogenization and did not result in any chemical transitions as no changes in mass was notable. The slight increment in weight observed from S2 (1109.89 ± 5.11mg) to S3 (1112.69 ± 4.89mg) could be associated with the effects of freezing on the co-particulate blend. Freezing can initiate solute-solute/solute-solvent/solvent-solvent intermolecular coalescence which can result in molecular packing and volumetric shrinkage leading to the generation of an orderly crystalline structure and an increase in mass and density of the frozen blend. Mass reduction from S3 (1112.69 ± 4.89mg) to S4 (568.50 ± 2.22mg) and finally S5 (175.30 ± 4.01mg) is related to the process of sublimation of the frozen solvent molecules leaving behind void air spaces (pores) within the matrix. A close relationship existed between the starting mass (S0: 181.50 ± 3.45mg) and the final mass of the P-RPM formulation (S5: 175.30 ± 4.01mg) indicative of the fact that the whole process is physical in nature and that matter was not created nor destroyed as no significant change of mass was observed.

6.3.1.1.4. Textural analysis of matrix physicomechanical strength

Table 6.4 presents the numerical values obtained for the matrix firmness (M_F) and energy of matrix distortion ($Є_D$) from the samples analyzed.

Table 6.4: Values of physicomechanical parameters measured utilizing samples generated during the preparation of the P-RPM formulation

Sample Description	M_F [a] (N/mm)	$Є_D$ [b] (J)
DMC [c]	1.029	0.062
WCD [d]	15.887	0.022
ECD [e]	9.087	0.031
N-CHB_{BC} [f]	20.591	0.014
N-CHB_{AC} [g]	22.616	0.012
P-RPM [h]	4.192	0.048

[a] M_F - matrix firmness, [b] $Є_D$ - the energy of matrix distortion, [c] DMC – dried mixture of constituting compounds before the initiation of the processes of fabrication [d] WCD – water-based co-particulate dispersion, [e] ECD – ethanol-based co-particulate dispersion, [f] N-CHB_{BC} - non-lyophilized co-particulate homogenous blend before curing, [g] N-CHB_{AC} - non-lyophilized co-particulate homogenous blend after curing, [h] lyophilized pore-regulated polymer matrix formulation

The result presented in Table 6.4 above revealed that the different phases of preparing the P-RPM formulation involved significant changes in physicomechanical measures. In this case, matrix firmness can be explained as the resistance of the matrix under study to the penetration of an external stress or force while the energy of distortion could be described as the energy dissipated to the external surroundings during the process of penetration. An inverse relationship exists between matrix firmness (M_F) and energy of matrix distortion ($Є_D$) implying that as matrix gets firmer or stiffer (i.e. increasing M_F), the energy of distortion reduces and vice versa. In other words, a firmer matrix may require higher energy levels to overcome intrinsic interactions responsible for matrix stiffness during the penetration of an external force. Consequently, lower energy magnitudes will be dissipated to the outer environment ($Є_D$).

With reference to Table 6.4, the loose powdered sample comprising the dry mixture of the constituting components and model drug (DMC) before the initiation of the whole process of constructing the P-RPM had the lowest M_F (1.029N/mm) and highest $Є_D$ (0.062J) which implies the resistance of the sample to penetration of the an external force was minimal resulting in the external dissipation of higher energy. Therefore, it can be inferred that the molecular interactions amongst the constituents of this sample were nominal. With the separate introduction of water (WCD) and ethanol (ECD), a significant increase in M_F (WCD: 15.887N/mm and ECD: 9.087N/mm) and $Є_D$ (WCD: 0.022J and ECD: 0.031J) was observed meaning that the addition of either water or ethanol moistened the surfaces of the powdered components possibly resulting in molecular swelling and inter-particulate interactions which would enhance co-particulate dispersion and generate a closely knitted solute-solvent network which could serve as a barrier to overcome by the application of an external force. The combination of WCD and ECD with the inclusion of Span 80 (surfactant) to form the non-lyophilized homogenous blend (Section 1.7 of Chapter 1) before curing (N-CHB_{BC}) resulted in an M_F (20.591N/mm) higher than those of WCD and ECD as well as an $Є_D$ (0.014J) lower than those of WCD and ECD. This implies that the combination of the WCD, ECD and Span 80 enhanced the formation of the stable, tightly networked un-lyophilized homogenous blend (before curing). Furthermore, curing of the homogenous blend (N-CHB_{AC}) appears to have some impact on enhancing matrix rigidity/stiffness as an increase in M_F (22.616N/mm) and a decrease in $Є_D$ (0.012J) was observed. Therefore, the curing process demonstrated the potential to enhance matrix entanglement and maintain an ordered porous matrix structure.

However, a sharp decline in M_F (4.192N/mm) and increase in $Є_D$ (0.048J) values obtained for the lyophilized P-RPM formulation was noted. This implies that the sublimation process that took place during lyophilization returned the matrix into its dry state but with some changes which is evidenced by the M_F (1.029N/mm) and $Є_D$ (0.062J) values of the DMC (dried compounds before initiating the fabrication process). Hence, the changes in the matrix network could be attributed to the introduction of the porous structure comprising of the pores and interconnectors which could serve as relevant barriers to mechanical penetration resulting in lower $Є_D$ and higher M_F values compared with the untreated mixture of constituting compounds (DMC). In short, the stages involved in the construction of the P-RPM formulation involved salient physicomechanical transitions.

6.3.1.2. Mechanism of action/performance

6.3.1.2.1. Assessment of possible structural deformations during the process of matrix performance

Comparatively varied spectral patterns were observed for the hydrated samples investigated with reference to the unhydrated P-RPM formulation (Figure 6.6).

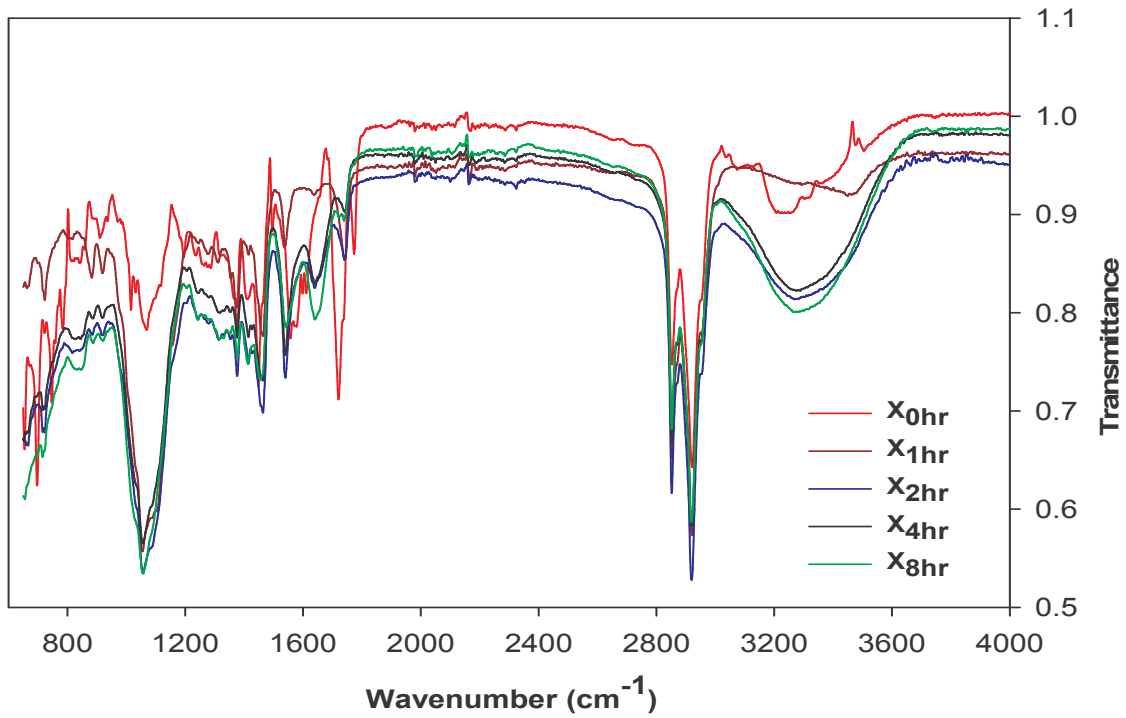

Figure 6.6: Superimposed FTIR spectra of the hydrated and unhydrated P-RPM formulations.

Table 6.5 presents the measured bands showing the shifts (with respect to the unhydrated P-RPM formulation, X_{0hr}) which occurred during the dissolution processes of the tested formulations (X_{1hr}, X_{2hr}, X_{4hr} and X_{8hr}). The observed band shifts presented in Table 6.5 may indicate that the hydration of the P-RPM formulation in simulated saliva perturbed the backbone of the matrix but did not bring about major cut off transitions. Band/peak shifts in this regard can refer to shifts/splitting/the elimination of existing ones. For instance, the bands due to OH, NH, NH_2, C-H, H-bonded NH_2 and OH stretching and O-C_2H_5 bending (3510 - 2854 cm^{-1}: X_{0hr}) gradually shifted to 3449 - 2852 cm^{-1} (X_{1hr}), 3275 - 2852 cm^{-1} (X_{2hr}), 3269 - 2852 cm^{-1} (X_{4hr}) and then 3268 - 2852 cm^{-1} (X_{8hr}). The vibrational frequencies observed between 3275 - 3268 cm^{-1} for X_{2hr}, X_{4hr} and X_{8hr} were broad banded (Figure 6.6). The immobilization of the weak C-H overtones present within the benzene ring of phenytoin sodium (2325 - 1982 cm^{-1}) was also displayed.

The band shifts displayed by all hydrated samples (X_{1hr}, X_{2hr}, X_{4hr} and X_{8hr}) in comparison to the reference sample (X_{0hr}) can be attributed to impact of the hydration process/dissolution conditions due to the formation of intramolecular hydrogen bonds between each sample and water molecules which aided the process of solvation/dissolution. Also, the presence of electrolytes ions within the dissolution medium (simulated saliva: disodiumhydrogenphosphate, potassium dihydrogenphosphate, sodium chloride and phosphoric acid) may initiate some level of reversible ionic bonds which may disturb the matrix network bringing about shifts in vibrational frequencies.

Overall, the P-RPM formulation can be described as stable and sturdy because, despite the progressive process of matrix hydration/dissolution, each tested matrix remnant retained the original chemical composition of the formulation. In other words, the constituting compound and the model drug did not appear to decompose through the process of hydration. This conclusion was made consequent to the fact that all analyzed remnants of hydrated samples in comparison to the unhydrated formulation generally retained the salient functional groups characteristic of the component compound and model drug which constituted the P-RPM formulation throughout the duration of hydration (Table 6.5).

Table 6.5: Shifts in the vibrational frequencies of relevant functional moieties of the hydrated samples with the unhydrated P-RPM formulation as a reference point

Vibrational Frequencies from Salient Functional Moieties	Formulation Description				
	X_{0hr} [a]	X_{1hr} [b]	X_{2hr} [c]	X_{4hr} [d]	X_{8hr} [e]
OH, NH, NH_2, stretching	3510	3449	-	-	-
	3232	3261	3275	3269	3268
C-H (cyclic or linear), H-bonded NH_2 and OH	3064	-	-	-	-
stretching and O-C_2H_5 bending	2924	2920	2920	2916	2918
	2854	2852	2852	2852	2852
Weak C-H overtones	2155	2162	2162	2325	
		2055			
	-	1982	1982	1982	1982
C=O, C=C stretching, -NH_3^+ and NH_2	1780	1741	1738	1741	1738
deformation and N-H bending	1724	1635	1640	1640	1640
COO^-, C-O-C, C-N stretching, C- OH bend,	1557	1539	1540	1540	1542
C-O^- and CH deformations	1445	1463	1463	1463	1455
		1413	1415	1415	1413
C-OH, C-O-C (acyclic), C-N stretching	1291	1374	1376	1376	1377
				1351	
	-	-	1314	1312	1310
	1082	1155	1240	1242	1240
		1072	1054	1057	1056
C-OH, NH deformations, O-C=O, N-C=O and	915	919	919	915	921
C-OH bending	789	882	883	879	887
	733	818	818	816	848
	-	723	717	723	713
	677	663	668	667	-

6.3.1.2.2. Evaluation of matrix surface morphology over the time of exposure

The scanning electron micrographs obtained for each hydrated sample in comparison with the unhydrated formulations were consistently changing as exposure time increased. Figure 6.7 illustrates these changes.

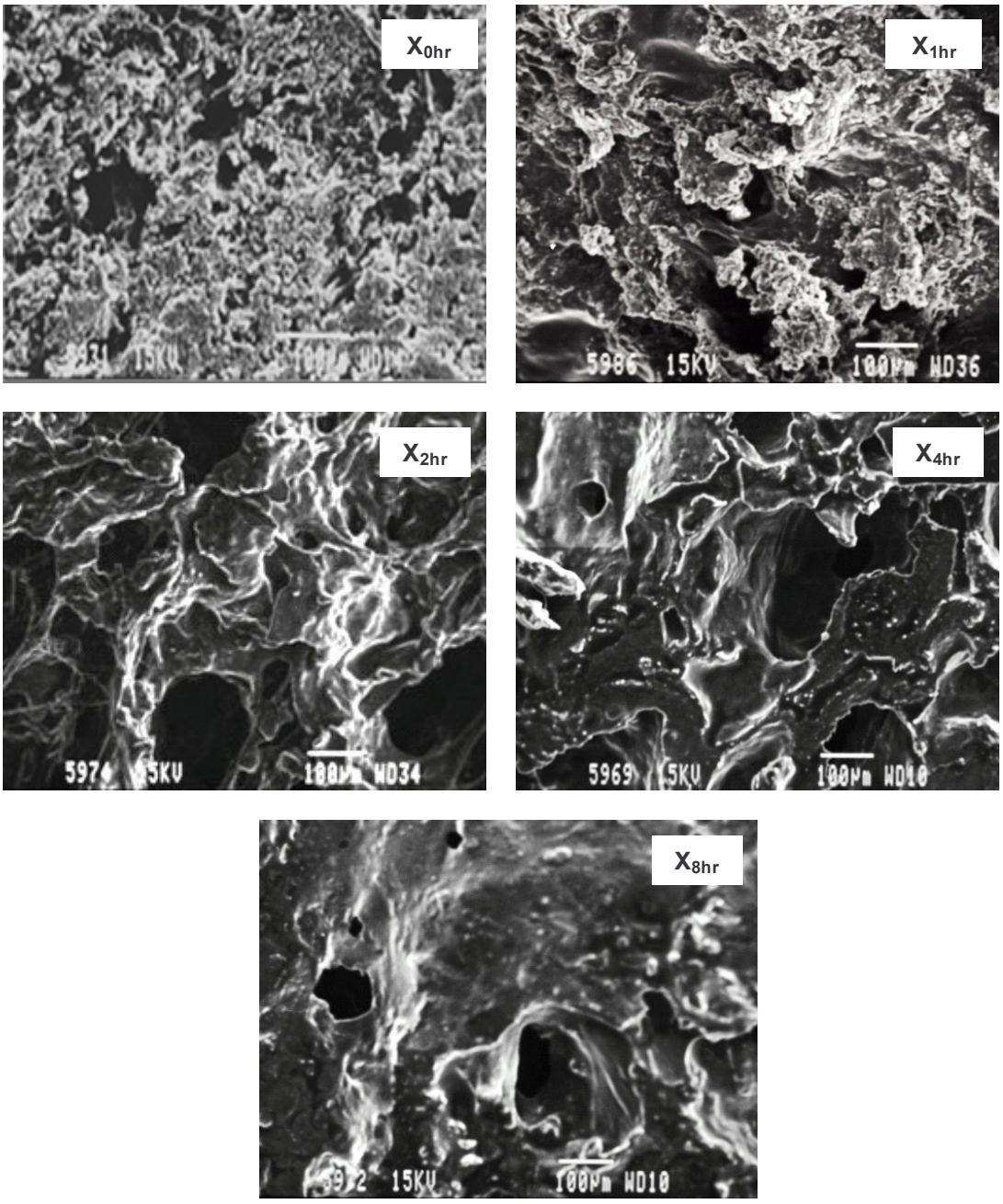

Figure 6.7: Scanning electron micrographs showing the changes in matrix surface geometry for the duration of hydration (magnification 1000×).

Micrographs displayed in Figure 6.7 above show that the porous network collapsed as the duration of exposure to the dissolution media increased. At the first hour (X_{1hr}), the well structured unhydrated porous structure (X_{0hr}) began to open up, pore interconnectors collapsed and larger undefined pores were formed. As hydration progressed to 2 hours of exposure (X_{2hr}), the porous network collapsed gradually and interconnectors merged and got less dense/transparent and more shapeless. Also, the formation of undefined globules due to the interactive influx of water molecules is notable at the second (X_{2hr}) and fourth hours (X_{4hr}). Furthermore, what can be described as gullies due to matrix erosion and collapse of the structured porous network was evident for X_{2hr}, X_{4hr} and X_{8hr}. At the eighth hour, a near complete collapse of porous structure was observed. Therefore, the hydration of the P-RPM formulation resulted in the collapse of its ordered porous network due to matrix disentangling which gradually results in progressive drug release and matrix dissolution.

6.3.1.2.3. Matrix gravimetric changes due to hydration

A consistent fractional matrix mass loss over the time of exposure to the dissolution media was observed. In other words, the remnant matrix reduced in gravimetric weight as the duration of hydration increased (Figure 6.8). This implies that the process of matrix hydration which initiated and maintained the collapse of the ordered matrix network (Figure 6.7) led to matrix solvation and overall mass loss as the time of exposure to the hydration media increased.

The relationship between the fractional drug release (Section 3.3.1.4.1 of Chapter three) and the fractional matrix loss using a graphical analysis are illustrated with Figure 6.9. The existence of a linear relationship (R^2 = 0.938) between fractional drug release and fractional mass loss is noteworthy. This indicates that the increase in fractional mass loss over the duration of exposure to the dissolution media equally results in an increase in the fraction of drug release over the same duration. Therefore, drug release from the P-RPM formulation is dependent on the hydration, extrication (collapse of the ordered porous structure) and dissolution of the matrix. It could be proposed that the drug molecules were entrapped and well distributed within the pores and interconnectors (porous structure) of the P-RPM formulation such that they could only be liberated when this porous network was disrupted.

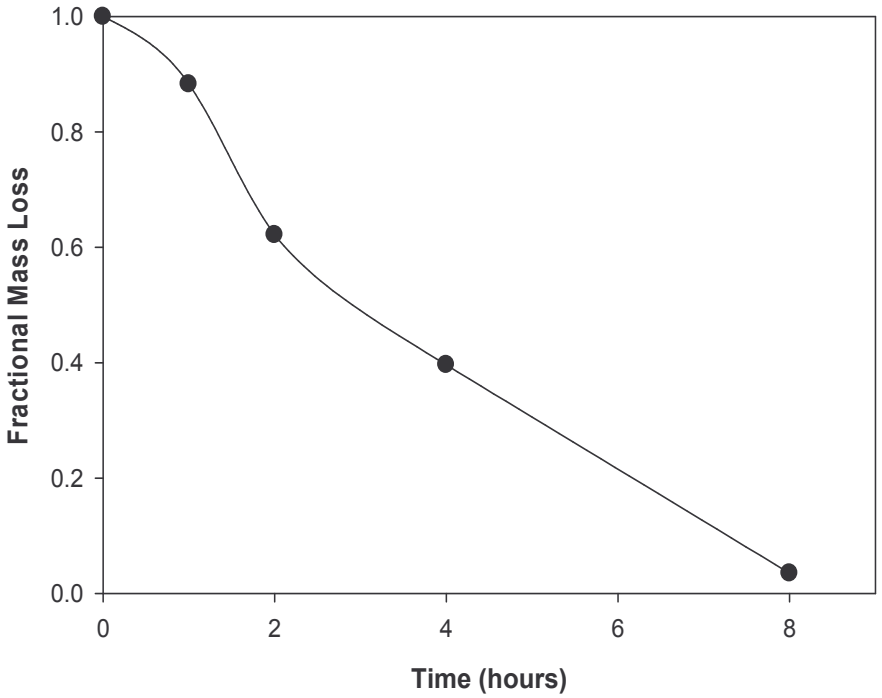

Figure 6.8: Changes in matrix fractional mass for the duration of exposure to the dissolution medium (n = 3 and Standard Deviation ≤ 0.02 in all cases).

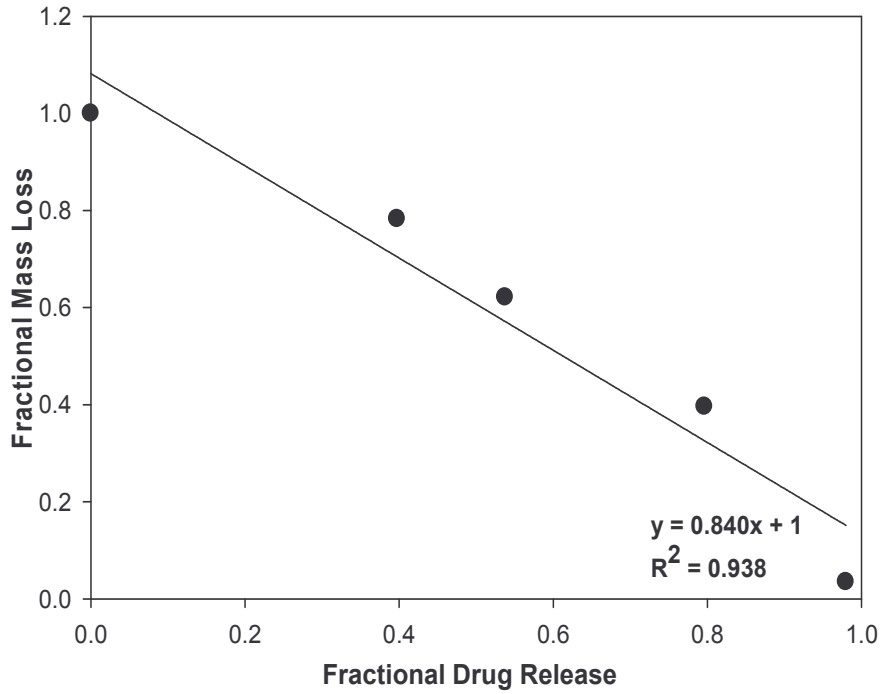

Figure 6.9: Linear relationship between fractional drug release and fractional mass loss.

6.3.1.2.4. Matrix textural alterations

The graphical representations of the changes in the values obtained for the matrix firmness (M_F) and energy of matrix distortion ($Є_D$) measurements are presented in Figures 6.10 (a) and (b) respectively. The transitions which occurred in the texture of the investigated samples are shown in Figure 6.11.

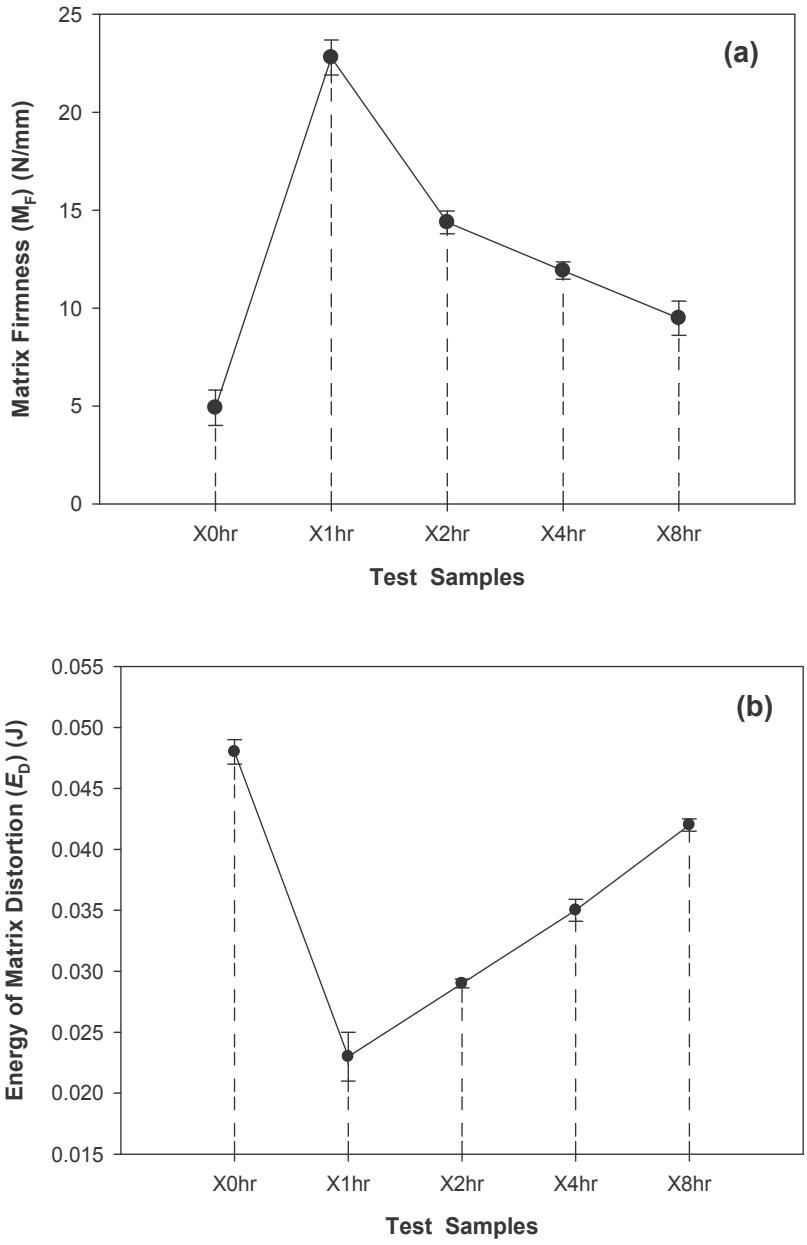

Figure 6.10: Changes in matrix physicomechanical strength due to hydration: (a) Matrix firmness and (b) Energy of matrix distortion.

The matrix firmness (M_F) which is a measure of rigidity or resistance to penetration by the externally applied force object increased in value at 1 hour hydration time (X_{1hr}) compared with the unhydrated P-RPM formulation (X_{0hr}). Subsequently, as the duration of hydration increased from 1 hour through to 8 hours, M_F decreased consistently but all obtained values for the hydrated samples were higher than that of X_{0hr}. Generally, the M_F values were higher for X_{1hr} to X_{8hr} (22.79 N/mm – 9.48 N/mm) relative to X_{0hr} (4.19N/mm). This may be attributable to matrix swelling as a result of hydration and plasticizing effects of water which can make the respective matrix more tortuous and resistant to penetration of an externally applied force. Also, the collapse of the matrix porous structure may be an augmenting factor to the overall increment in M_F values observed for the hydrated sample compared with the unhydrated one.

However, the consistent decrease in M_F values observed amongst the hydrated samples (X_{1hr} – X_{8hr} : 22.79 N/mm – 9.48 N/mm) can be as a result of matrix erosion as the time of exposure to the dissolution media increased. Therefore, as the matrix hydration progressed, erosion occurred concomitantly resulting in a reduction in the degree of matrix entanglement. Consequently, the force of penetration reduces as the matrix barrier capacity, penetration distance are minimized and porous structure disrupted due to matrix gravimetric loss resulting in the decrease in M_F. This proposition is further fortified by the illustration in Figure 6.11 as the penetration force and distance decreased as hydration time increased from X_{1hr} to X_{8hr}.

The energy of matrix distortion ($Є_D$) (a measure of energy dissipated to the environment) on the other hand increased from X_{1hr} to X_{8hr} (0.023 J to 0.0042 J) indicating that more energy is liberated to the environment during the application of an external force as the energy expended to overcome intra-matrix barriers due to the disruption of the ordered porous network, matrix disentanglement and swelling is less as hydration time progresses as a result of matrix loss. Nevertheless, the magnitude of $Є_D$ for the unhydrated matrix was highest (0.048 J) indicative of an ordered porous structure, intact, dry and compact matrix. Consequently, this matrix presents with minimal hindrances to penetration resulting in a reduction in the magnitude of performed worked and an elevation in the level of energy dissipated to the environment.

The changes in matrix porosity depicted by the undulating peaks in Figure 6.11 were computed as a textural quantity described as “average drop offs” (red and green arrows). It was observed that the values dropped from 15.48 (for the unhydrated matrix, X_{0hr}) to 2.58 (X_{1hr}), 0.89 (X_{2hr}),

0.16 (X_{4hr}) and 0.08 (X_{8hr}) upon hydration. This further substantiates the relationship between matrix hydration, porosity and physicomechanical transitions as well as the surface morphology and other quantitative changes.

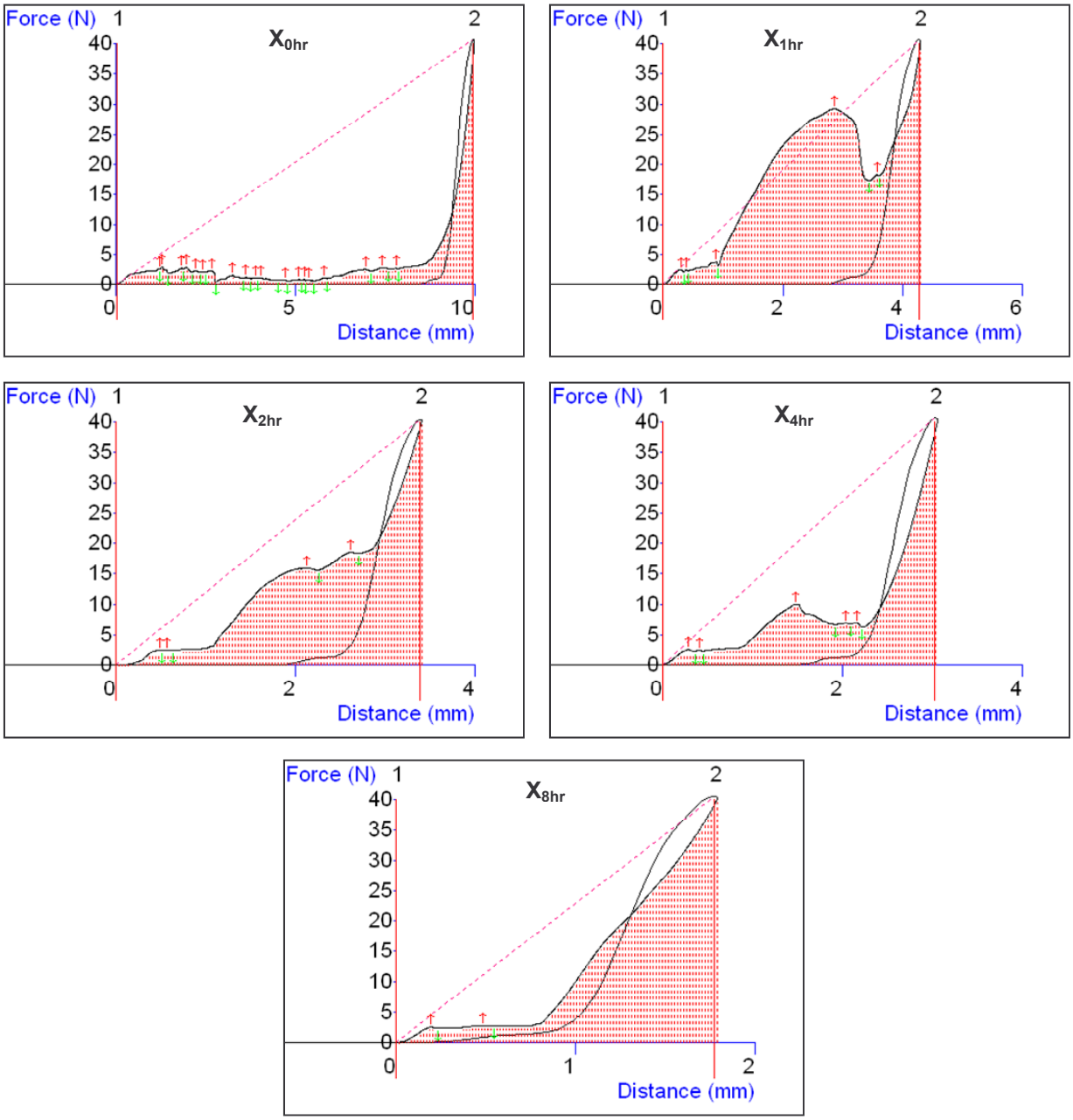

Figure 6.11: Profiles showing the changes in matrix texture over time due to hydration.

6.3.2. The application of computational modeling to elucidating the mechanisms of configuration and function of the P-RPM formulation

6.3.2.1. Prediction of the mechanism of formation/configuration

Generated computational models showed that the formation of the homogenous blend was initiated by solute (polymeric, non-polymeric and drug compounds) and solvent (ethanol and water) interactive dispersions which gave rise to hydrophilic pockets with different polymeric and non-polymeric strand associations as well as dispersed water, ethanol and drug molecules within the matrix. The drug molecules were located in close proximity to the hydrophilic pockets and in close association with other polymeric, non-polymeric, aqueous and ethanolic components. Also, the drug molecules displayed particular interactions with gelatin molecules which may be attributed to its high level of hydrophilicity (Figure 6.12).

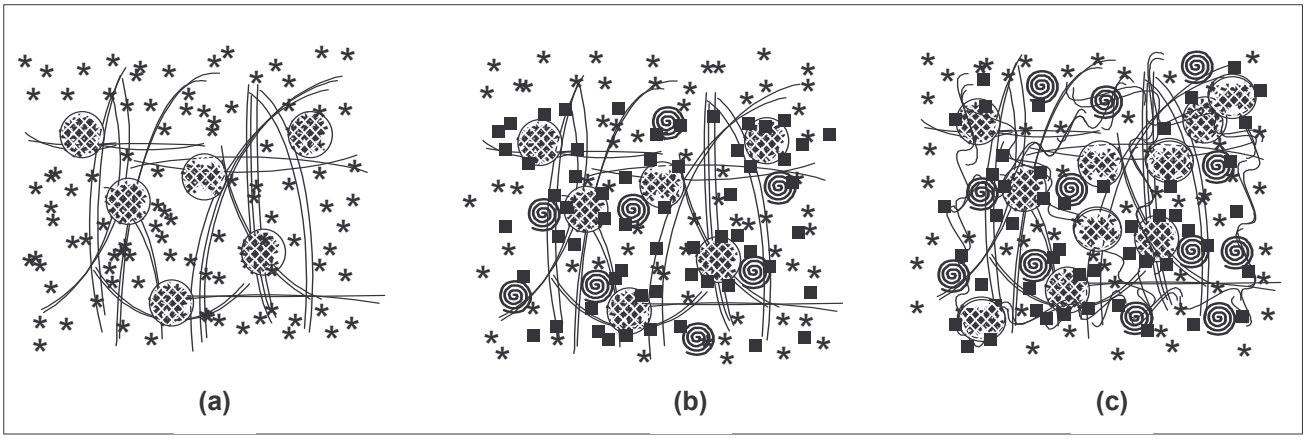

Figure 6.12: A computationally modeled illustration of the processes of formation of the drug-loaded homogenous co-particulate blend showing: (a) different polymer's strands, scattered solvent molecules (stars) in independent hydrophilic interactions, (b) the presence of the drug molecules (squared dots), associations of drug with the gelatin molecules (eccentric circular dots) and solutes particles in the mixed medium containing ethanol (free space/void), (c) a drug loaded homogenous blend before freeze-drying.

Interactions between the solute components and water-ethanol solvent medium were prominent and mainly of the hydrophilic type. This resulted in the formation of solute-solvent dispersions due to layering of the solvent components. Hydrophilic-natured pockets developed around

carboxyl and hydroxyl entities of the polymeric and non-polymeric solute components without strand twisting which are indicative of physical, non-destructive transitions (Figure 6.13).

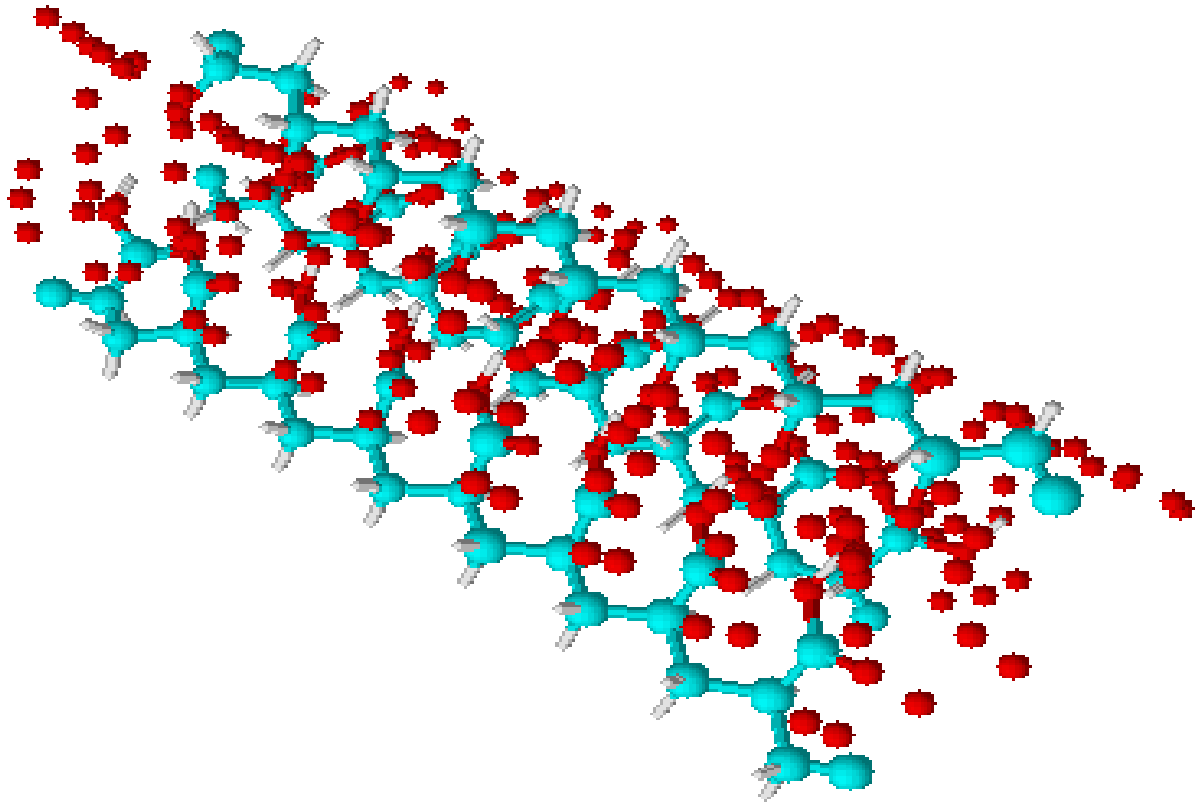

Figure 6.13: A computationally modeled three-dimensional mesh showing interaction between the solvent centres (red circles) and solute strands (greenish circles) forming hydrophilic-natured pockets (off-white spaces).

It was noted that solute-solvent interactions occurred in different orientations with some areas showing higher solvent clusters than some other regions due to the varying affinities of the solute centres and drug molecules for the solvent functional groups (Figure 6.14).

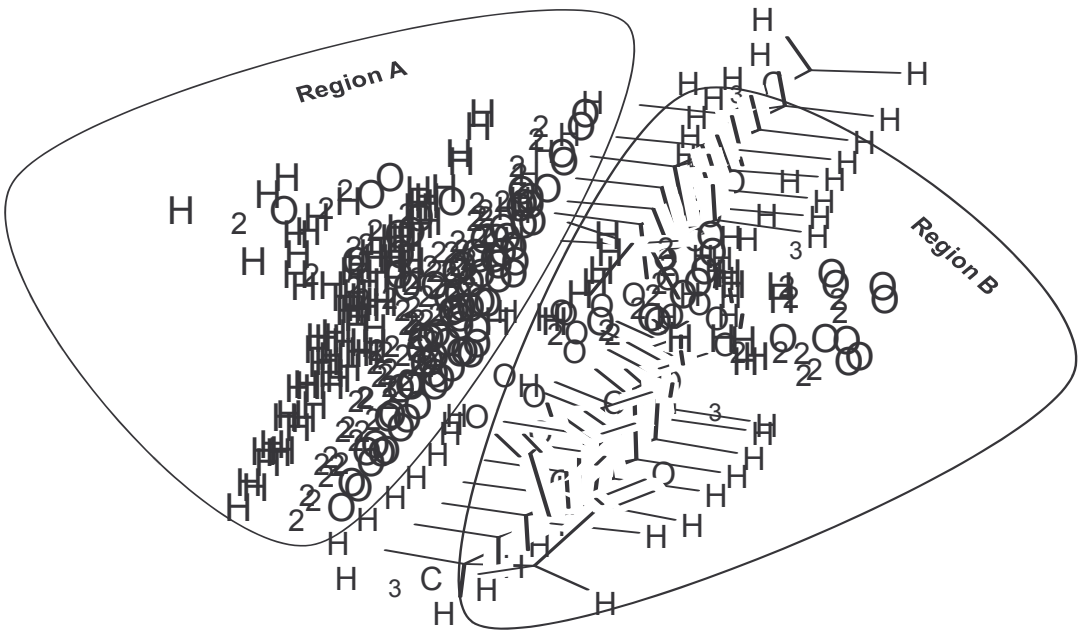

Figure 6.14: Computationally modeled depiction of layering due to strong hydrophilic solute-solvent interactions (Region A) and scattered solvent molecules (Region B) around lesser affinity groups, molecules, polymers and drugs.

The generated model was able to visualize the formation of single and multiple cavities resulting from the associative physicochemical interactions between the solute and solvent molecules within the homogenous blend milieu (Figure 6.15). These cavities appear to be prerequisites to the formation of the pore structures as well as possibly functioning as interfaces for the attachment of drug molecules. Furthermore, the multiple cavities were observed to be associated with the multiple solute strand interaction giving rise to inter-strand cavities (Figure 6.16).

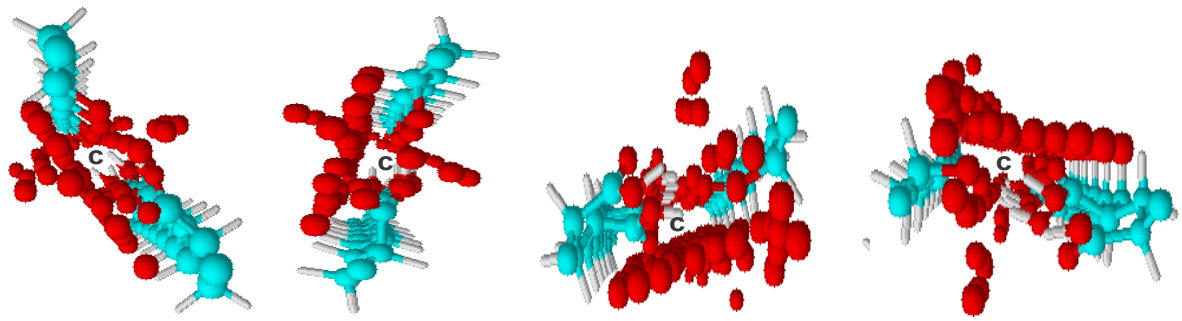

Figure 6.15: Computationally modeled representation of solute-solvent interactions resulting in the formation of cavities (off-white, asymmetric circular portions within the network labeled ‘c’).

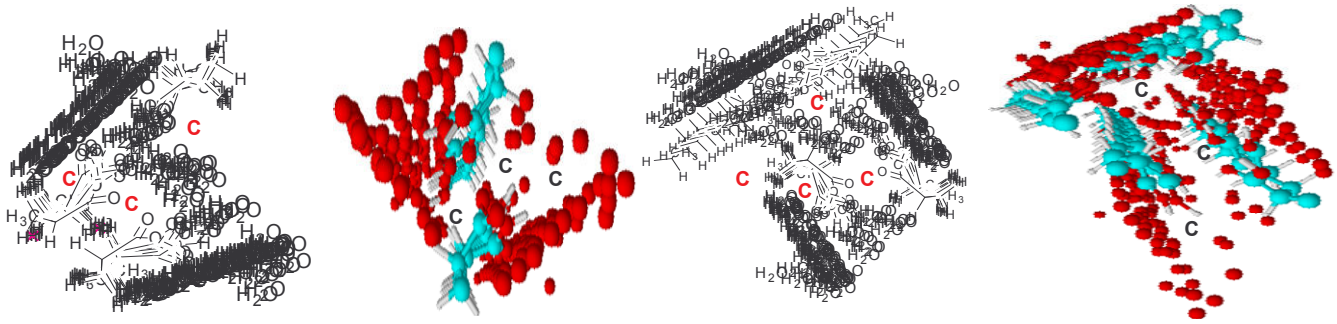

Figure 6.16: Computationally modeled illustration of multiple solute strands in interaction with solvent molecules resulting in the evolution of inter-strand, multiple cavities (labeled ‘c’).

In addition, the model showed that interconnection of the multiple cavities occurred and this resulted from the multiple solute strands undergoing multi-link physicochemical interactions along with the drug molecules to form channels (in the angstrom size range) indicative of the ordered porous structure (including the pores and interconnectors) of the P-RPM matrix (Figure 6.17).

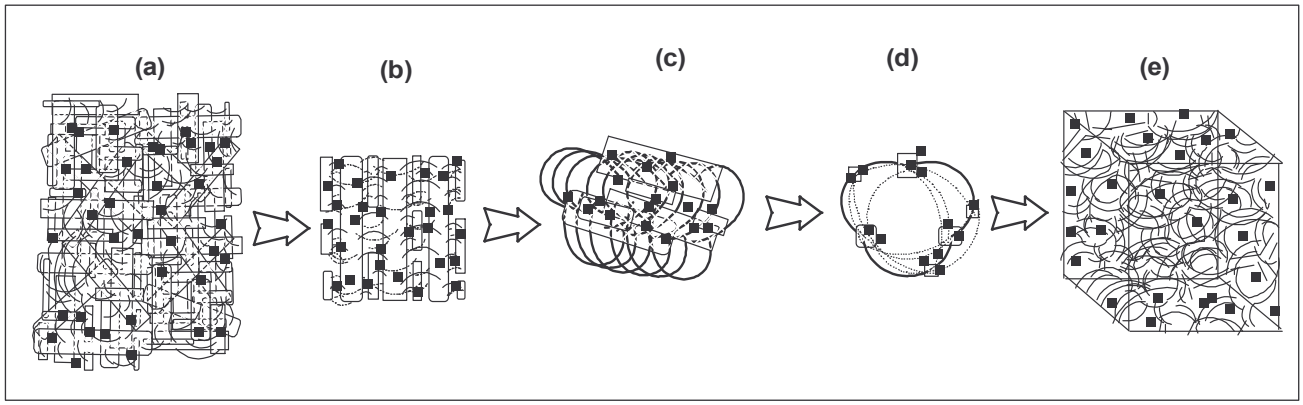

Figure 6.17: A computationally modeled schematic showing the formation of interconnected cavities forming the channels: (a) drug-loaded, homogenized blend, (b) multiple strands undergoing physicochemical interactions along with drug molecules (as squared dots), (c) physicochemical interactive associations (represented as broken and solid lines) between solute-solute strands interconnectors, (d) a foot-print view of the associations and channel cavity and (e) a three-dimensional view of inter-strand networked channels (ordered porous structure) with drug molecules loaded unto the matrix.

Overall, the schematic in Figure 6.18 (a) – (d) summarizes the stages involved in the fabrication of the ordered porous matrix.

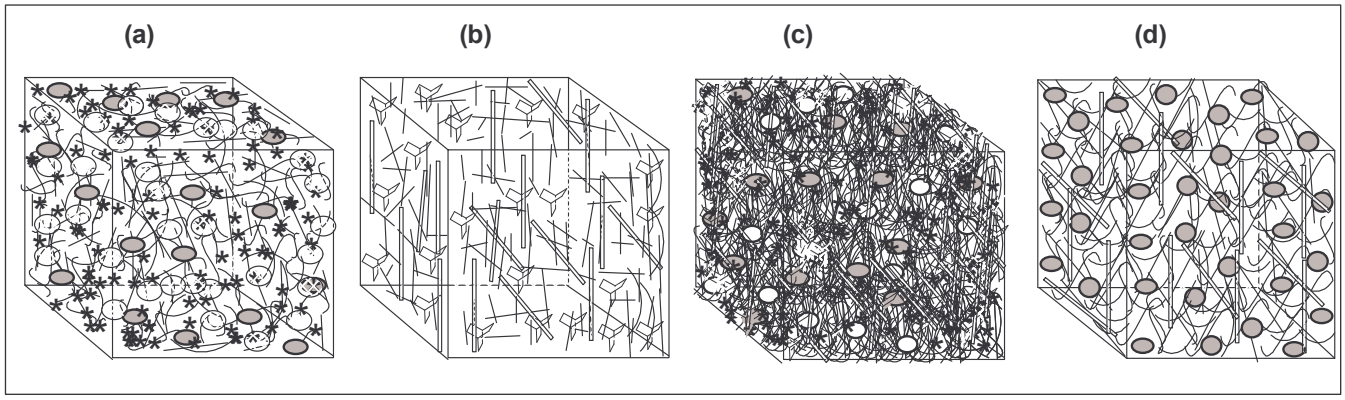

Figure 6.18: Computational models showing the construction of the drug loaded P-RPM formulation: (a) drug loaded water-based co-particulate dispersion showing several solute strands, drug molecules (grey circles) undergoing hydrophilic physicochemical interactions (white circles) and molecules of the water (star-shaped entities) scattered within the matrix, (b) the ethanol based co-particulate dispersion with the solutes depicted as broken lines and elongated double lines, ethanol molecules as y-shaped figurines scattered in the preparatory matrix, (c) a mixture of (a) and (b) with span 80 (reduction of interfacial tension) to form the homogenous co-particulate blend characterized by as increased volume density of the constituents, (d) the freeze-dried or lyophilized matrix devoid of free floating water, water pockets, ethanol and ethanol-water associative entities which gave rise to a homogenized and ordered porous matrix showing solute strands from both the water-based and ethanol-based co-particulate dispersions origins as well as evenly distributed drug molecules and other associated adds-up of the blend (physical interaction).

6.3.2.2. Proposed mechanism of performance/action

Computational modeling predicted that the P-RPM matrix functioned basically by undergoing a compressive break-up of the ordered matrix porous structure. This process is depicted in Figure 6.19.

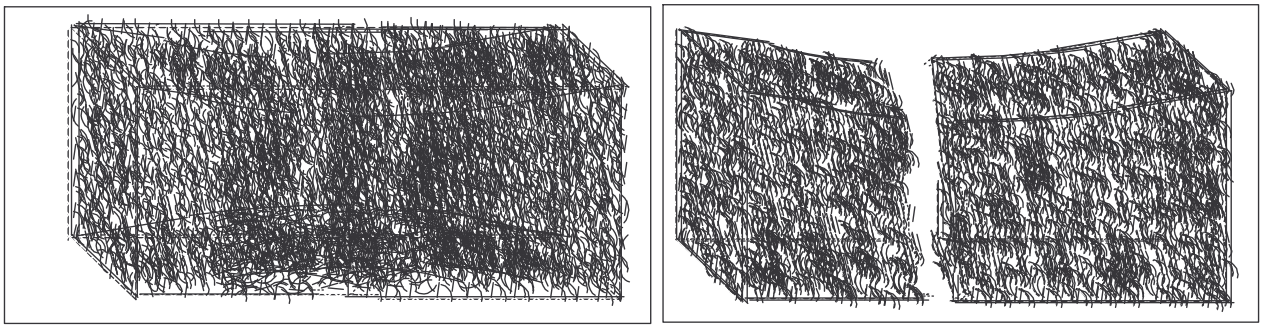

Figure 6.19: A computationally modeled compressive disruption of the ordered porous structure.

6.3.2.3. Energy paradigms

Significant changes in energy during the formation and performance of the P-RPM formulation were observed. The internal energy (E) was higher for the porous matrix formulation than for the homogenous blend. This is indicative of a stable, less disturbed porous matrix with minimal entropy changes (Figure 6.20 (a)). The process of porous matrix breakdown was characterized by regressive energy decay over time which can be related to a reduction in matrix stability due to disentanglement and an increase in system entropy (degree of randomness) (Figure 6.20 (b)).

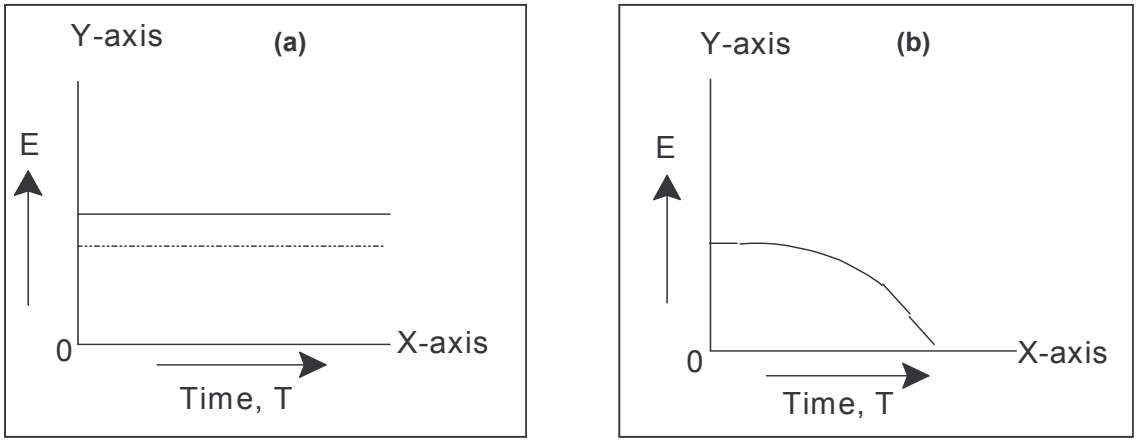

Figure 6.20: The: (a) Qualitative representation of averaged typical energy, E against time, T of the porous matrix (solid line) and energy of the homogenized blend (broken lines), (b) Energy decay over time in a regressive pattern.

6.4. CONCLUDING REMARKS

This section attempted to elucidate the underlying mechanisms potentially guiding the construction and performance of the novel P-RPM formulation under investigation using both experimental and computationally modeled processes. The experimental approach revealed that the methodical phases of fabricating the P-RPM formulation were based on structurally non-destructive physical and mechanical procedural transitions and that the overall performance of the formulation was due to the contributive effects/properties of the constituting compounds. In addition, the mechanism of action/function of the P-RPM formulation was attributable to the disruption of the ordered porous matrix structure by physical processes such as disentangling, matrix swelling, plasticization and dissolution due to hydration with simulated saliva. This process also had significant impact on the physicomechanical strength of the P-RPM formulation but the formulation retained its physicochemical stability as hydration progressed. Furthermore, the outcome of the computational molecular modeling correlated and substantiated the findings of the experimental procedures. In the subsequent chapter, preliminary lead investigations will be conducted to evaluate the impact of scale-up processes and relevant environmental storage conditions on the general physicochemical and physicomechanical characteristics as well as stability of the P-RPM formulation.